Syntheses, structures and luminescence properties of lanthanide coordination polymers with helical character

Rui-Sha Zhou, Xiao-Bing Cui, Jiang-Feng Song, Xiao-Yu Xu, Ji-Qing Xu *, Tie-Gang Wang

College of Chemistry and State Key Laboratory of Inorganic Synthesis and Preparative Chemistry, Jilin University, Changchun, Jilin 130021, P.R. China

ARTICLE INFO

ABSTRACT

A series of lanthanide coordination polymers, $(Him)_n[Ln(ip)_2(H_2O)]_n$ [Ln = La(**1**), Pr(**2**), Nd(**3**) and Dy(**4**), H_2ip = isophthalic acid, im = imidazole] and $[Y_2(ip)_3(H_2O)_2]_n \cdot nH_2O$ (5), have been synthesized and characterized by elemental analyses, infrared (IR), ultraviolet-visible-near infrared (UV-Vis-NIR) and single-crystal X-ray diffraction analyses. The isostructural compounds **1–4** possess 3-D structures with three different kinds of channels. Compound **5** features a 2-D network making of two different kinds of quadruple-helical chains. Compounds **2** and **3** present the characteristic emissions of Pr(III) and Nd(III) ions in NIR region, respectively. Compound **4** shows sensitized luminescence of Dy(III) ions in visible region.

1. Introduction

Investigations on the construction of coordination polymers have attracted great interests not only for their intriguing architectures and topologies but also for their applications in areas of catalysis, sorption, separation, luminescence, magnetism, nonlinear optical property, etc. [1–5]. A variety of coordination polymers with diversified topologies and interesting properties have been prepared through judicious choice of metal centers and organic linkers. As functional metal centers, lanthanide metals have received more and more attention for their special coordination properties and peculiar luminescent and magnetic properties. The desire to prepare novel topological networks has motivated researchers to employ lanthanides with high coordination numbers and flexible coordination geometries as metal centers to assemble coordination polymers [6,7]. With respect to luminescence, the emissions from near infrared (NIR) radiation to blue light of different lanthanide ions make them of interest for a range of applications. The NIR luminescence from Nd-containing system, for example, has been regarded as the most popular infrared luminescence materials for application in laser systems [8]. However, direct excitation of the $4f$–$4f$ transitions is difficult because of poor absorption abilities of lanthanides. Efficient excitation of the metal-centred luminescence has to rely on energy transfer from the surroundings of the lanthanide ion [9].

Thus, the selection of a suitable ligand is crucial in the building of lanthanide coordination polymers. Isophthalic acid possesses excellent characteristics as follows: (i) it has two carboxyl groups with four oxygen atoms which can be used for coordination; (ii) the skew coordination orientation of the carboxyl groups should favor the formation of a helical structure [10,11] and (iii) its phenyl group having high structuring effect could act as efficient sensitizer for lanthanide emissions [9]. Imidazole, an organic diamine ligand, can act as template molecules or structure-directing agents to yield new coordination polymers.

So far, some lanthanide coordination polymers being constructed by ip and a secondary ligand (such as 2, 2′-bipy, phen and acetate) [15–19] and several lanthanide coordination polymers containing ip-only ligands (no containing other organic constituents) [12–14] have been investigated. However, to the best of our knowledge, none of the compounds constructed by lanthanides, ip and imidazole ligands have been reported. On the basis of the aforementioned points, we attempt to employ lanthanide ions, isophthalic acid and imidazole ligands to assemble new compounds. Fortunately, we obtained four isostructural 3-D coordination polymers with three different kinds of helical channels, $(Him)_n[Ln(ip)_2(H_2O)]_n$ [Ln = La(**1**), Pr(**2**), Nd(**3**) and Dy(**4**), H_2ip = isophthalic acid, im = imidazole]. It should be mentioned that examples of the structure containining three different kinds of channels are rare in reported relevant literatures so far, and these compounds may have potential applications in heterogeneous asymmetric catalysts and chiral separations [20]. We also obtained a 2-D layer coordination polymer, $[Y_2(ip)_3(H_2O)_2]_n \cdot nH_2O$ (**5**), with two different kinds of quadruple-helical chains with

different helicities. In addition, we also report here the luminescence properties of compounds **2–4**.

2. Experimental section

2.1. Material and methods

All chemicals purchased were of reagent grade and used without further purification. Elemental analyses (C, H and N) were performed on a Perkin-Elmer 240C elemental analyzer (USA). Infrared (IR) spectra were measured on a Perkin-Elmer Spectrum One FT-IR spectrometer (USA) using KBr pellets. The NIR luminescence spectra of compounds **2** and **3** were obtained at room temperature on a BIO-RAD PL9000 Photoluminescence System (UK) with an Ar ion laser and the Ge detector worked at liquid nitrogen temperature. The visible luminescence spectrum of compound **4** was measured on a Perkin-Elmer LS55 spectrometer (USA).

2.2. Syntheses

Compounds **1–5** were prepared under hydrothermal conditions. Mixtures of lanthanide salts [La(NO$_3$)$_3$·6H$_2$O (0.22 g, 0.5 mmol) for **1**, Pr(NO$_3$)$_3$·6H$_2$O (0.22 g, 0.5 mmol) for **2**, Nd(NO$_3$)$_3$·6H$_2$O (0.22 g, 0.5 mmol) for **3**, Dy(NO$_3$)$_3$·6H$_2$O (0.23 g, 0.5 mmol) for **4** and Y(NO$_3$)$_3$·6H$_2$O (0.19 g, 0.5 mmol) for **5**], H$_2$ip (0.17 g, 1 mmol), im (0.03 g, 0.5 mmol), C$_2$H$_5$OH (5 ml) and water (15 ml) were stirred for ca. 2 h and the pH values of reaction system were controlled in the range 3–4 by addition of 0.2 mol l^{-1} nitric acid, then the mixtures in 25 ml Teflon-lined stainless steel vessels were heated under autogenous pressure at 160 °C for 72 h and finally cooled to room temperature. Colorless polyhedron crystals of **1** and **4**, pale-green polyhedron crystals of **2**, pale-violet polyhedron crystals of **3** and colorless club-shaped crystals of **5** were filtered, washed with distilled water and dried at ambient temperature. Yield: 0.12 g (43.30%, based on lanthanum) for **1**; 0.16 g (57.53%, based on praseodymium) for **2**; 0.19 g (67.90%,

based on neodymium) for **3**; 0.11 g (38.07%, based on dysprosium) for **4**; 0.05 g (27.62%, based on yttrium) for **5**. Analysis calculated (Anal. Calcd) for C$_{19}$H$_{15}$LaN$_2$O$_9$ (554.24), **1**: C, 41.14; H, 2.71; N, 5.05%. Found: C, 41.36; H, 2.69; N: 4.93%.

Anal. Calcd for C$_{19}$H$_{15}$PrN$_2$O$_9$ (556.24), **2**: C, 40.99; H, 2.69; N, 5.03%. Found: C, 40.81; H, 2.58; N, 4.90%.
Anal. Calcd for C$_{19}$H$_{15}$NdN$_2$O$_9$ (559.57), **3**: C, 40.75; H, 2.68; N, 5.00%. Found: C, 40.58; H, 2.67; N, 4.90%.
Anal. Calcd for C$_{19}$H$_{15}$DyN$_2$O$_9$(577.83), **4**: C, 39.46; H, 2.59; N, 4.85%. Found: C, 39.61; H, 2.53; N, 4.73%.
Anal. Calcd for C$_{24}$H$_{18}$Y$_2$O$_{15}$ (724.20), **5**: C, 39.77; H, 2.49%. Found: C, 39.87; H. 2.44%.

2.3. X-ray crystallography

The crystal structures were determined by single-crystal X-ray diffraction analyses. The data were collected on a Bruker-AXS Smart CCD diffractometer (Mo $K\alpha$, $\lambda = 0.71073$ Å) at room temperature with ω-scan mode. The structures were solved by direct methods and refined by full-matrix least squares on F^2 using SHELXTL 97 software [21]. Non-hydrogen atoms were refined anisotropically. The hydrogen atoms were located from differences Fourier maps and refined with isotropic temperature factors in compounds **1–5**. All calculations were carried out using SHELXTL 97 [21] and PLATON 99 [22]. The crystallographic data and pertinent information are summarized in Table 1. The selected bond lengths are listed in Table 2.

3. Results and discussion

3.1. Syntheses

The hydrothermal method has been proved to be very effective for the syntheses of coordination polymers. It is well known that small changes in one or more of reaction factors, such as pH value, temperature, reaction time, molar ratio of the reactants, etc.,

Table 1
The crystallographic data for compounds **1–5**

Compound	1	2	3	4	5
Empirical formula	C$_{19}$H$_{15}$LaN$_2$O$_9$	C$_{19}$H$_{15}$N$_2$PrO$_9$	C$_{19}$H$_{15}$N$_2$NdO$_9$	C$_{19}$H$_{15}$DyN$_2$O$_9$	C$_{24}$H$_{18}$O$_{15}$Y$_2$
Formula weight	554.24	556.24	559.57	577.83	724.20
Crystal system	Orthorhombic	Orthorhombic	Orthorhombic	Orthorhombic	Monoclinic
Space group	*Pnna*	*Pnna*	*Pnna*	*Pnna*	*P*2$_1$/*c*
a/Å	9.5277 (13)	9.5051 (6)	9.5107 (2)	9.4300 (15)	10.594 (2)
b/Å	14.692 (2)	14.6243 (10)	14.6128 (3)	14.480 (2)	14.216 (3)
c/Å	13.6772 (18)	13.5603 (9)	14.191 (3)	13.306 (2)	17.150 (4)
β/deg	90	90	90	90	97.962 (4)
V (Å)	1914.5 (4)	1885.0 (2)	1880.61 (7)	1816.9 (5)	2558.1 (10)
Z	4	4	4	4	4
ρ_{calc}/g cm^{-3}	1.923	1.960	1.976	2.112	1.880
Absorption coef./mm^{-1}	2.290	2.644	2.820	4.174	4.593
θ range (deg)	2.03–26.05	2.05–26.01	2.05–25.00	2.65–26.05	1.87–26.13
Reflections collected	9937	9813	10969	14460	14168
Unique reflections (*R*int)	1869 (0.0420)	1861 (0.0204)	2150 (0.0831)	1799 (0.1049)	5059 (0.0671)
Completeness	99.9%	99.9%	100.0%	99.9%	99.3%
Goodness-of-fit on F^2	1.089	1.102	1.073	1.068	0.950
R indexes [$I>2\sigma(I)$][a]	R1 = 0.0190, wR2 = 0.0486	R1 = 0.0173, wR2 = 0.0426	R1 = 0.0264, wR2 = 0.0716	R1 = 0.0259, wR2 = 0.0621	R1 = 0.0452, wR2 = 0.0807
R (all data)[a]	R1 = 0.0228, wR2 = 0.0503	R1 = 0.0205, wR2 = 0.0449	R1 = 0.0310, wR2 = 0.0746	R1 = 0.0299, wR2 = 0.0650	R1 = 0.0806, wR2 = 0.0918
Largest diff. peak and hole (e/Å^{-3})	0.377, −0.512	0.316, −0.506	0.970, −1.345	1.306, −1.701	0.700, −0.419

[a] $R_1 = \Sigma||F_0|-|F_c||/\Sigma|F_0|$; $wR = [\Sigma w(F_0^2-F_c^2)_2/\Sigma w(F_0^2)^2]^{1/2}$.

Table 2
Selected bond lengths (Å) for 1–5

			1[a]		
La(1)–O(2)#1	2.425 (2)	La(1)–O(3)#3	2.436 (2)	La(1)–O(4)#5	2.699 (2)
La(1)–O(2)#2	2.425 (2)	La(1)–O(5)#4	2.609 (1)	La(1)–O(4)#4	2.699 (2)
La(1)–O(3)	2.436 (2)	La(1)–O(5)#5	2.609 (1)	La(1)–O(1W)	2.718 (4)
			2[b]		
Pr(1)–O(2)#1	2.382 (2)	Pr(1)–O(3)	2.393 (2)	Pr(1)–O(4)#5	2.668 (2)
Pr(1)–O(2)#2	2.382 (2)	Pr(1)–O(5)#4	2.572 (1)	Pr(1)–O(4)#4	2.668 (2)
Pr(1)–O(3)#3	2.393 (2)	Pr(1)–O(5)#5	2.572 (1)	Pr(1)–O(1W)	2.681 (3)
			3[c]		
Nd(1)–O(2)#1	2.378 (2)	Nd(1)–O(3)	2.391 (2)	Nd(1)–O(4)#4	2.659 (2)
Nd(1)–O(2)#2	2.378 (2)	Nd(1)–O(5)#4	2.564 (2)	Nd(1)–O(4)#5	2.659 (2)
Nd(1)–O(3)#3	2.391 (2)	Nd(1)–O(5)#5	2.564 (2)	Nd(1)–O(1W)	2.674 (5)
			4[d]		
Dy(1)–O(2)#1	2.287 (2)	Dy(1)–O(3)#3	2.303 (2)	Dy(1)–O(1W)	2.594 (4)
Dy(1)–O(2)#2	2.287 (2)	Dy(1)–O(5)#4	2.484 (2)	Dy(1)–O(4)#4	2.604 (2)
Dy(1)–O(3)	2.303 (2)	Dy(1)–O(5)#5	2.484 (2)	Dy(1)–O(4)#5	2.604 (2)
			5[e]		
Y(1)–O(12)#5	2.221 (3)	Y(1)–O(6)	2.366 (3)	Y(2)–O(10)	2.332 (3)
Y(1)–O(7)#1	2.259 (3)	Y(1)–O(14W)	2.373 (4)	Y(2)–O(5)	2.394 (3)
Y(1)–O(4)#4	2.275 (3)	Y(2)–O(3)#4	2.271 (3)	Y(2)–O(2)	2.425 (3)
Y(1)–O(13W)	2.298 (4)	Y(2)–O(8)#1	2.280 (3)	Y(2)–O(1)	2.495 (3)
Y(1)–O(9)#2	2.351 (3)	Y(2)–O(11)#2	2.280 (3)	Y(2)–O(6)	2.641 (3)

[a] Symmetry codes for compound **1**: #1 −x+2, −y, −z; #2 x+1/2, y, −z; #3 −x+5/2, −y, z; #4 x,−y+1/2,−z+1/2; #5 −x+5/2, y−1/2, −z+1/2.
[b] Symmetry codes for compound **2**: #1 −x+2, −y, −z+1; #2 x+1/2, y, −z+1; #3 −x+5/2, −y, z; #4 x, −y+1/2, −z+3/2; #5 −x+5/2, y−1/2, −z+3/2.
[c] Symmetry codes for compound **3**: #1 −x, −y+1, −z; #2 x+1/2, y, −z; #3 −x+1/2, −y+1, z; #4 −x+1/2, y+1/2, −z+1/2; #5 x, −y+1/2, −z+1/2.
[d] Symmetry codes for compound **4**: #1 x+1/2, y, −z; #2 −x, −y+1, −z; #3 −x+1/2, −y+1, z; #4 −x+1/2, y+1/2, −z+1/2; #5 x, −y+1/2, −z+1/2.
[e] Symmetry codes for compound **5**: #1 −x+1, y−1/2, −z+1/2; #2 −x+1, y+1/2, −z+1/2; #3 x, y−1, z; #4 −x, −y+1, −z; #5 x, y+1, z.
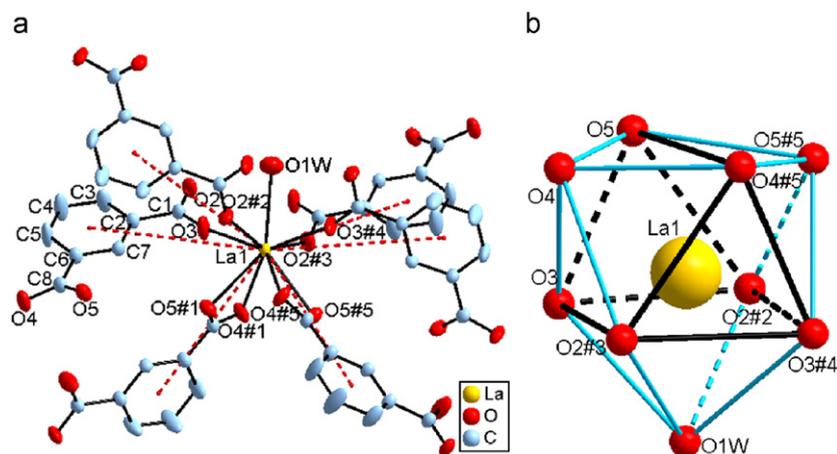

Fig. 1. (a) Coordination environment of La(III) in **1**. Thermal ellipsoids are at 50% probability. Dashed lines illustrate the six-connected circumstance of the La(III) node. (b) The distorted tricapped trigonal prism coordination polyhedron of the La(III) ion of compound **1**. Symmetry codes: #1, x, 0.5−y, 0.5−z; #2, 0.5+x, y, −z; #3, 2−x, −y, −z; #4, 2.5−x, −y, z; #5, 2.5−x, −0.5+y, 0.5−z.

sometimes may result in profound influence on final reaction products.

Compounds **1**–**4** were successfully prepared with good yields through hydrothermal reaction at the pH values of 3–4. When the pH values of reaction systems were 5–6 and other reaction conditions being unchanged, crystal products of compounds **1**–**4** with lower yields were obtained, while pH = 7–8 powder products were obtained, which were proven to be compounds **1**–**4**, respectively, by their IR spectra.

We also tried to prepare Y(III) analog of compounds **1**–**4** under a similar condition, but we only obtained compound **5** without im ligand. When the im ligand was not added to the reaction system, no crystals of **5** were obtained. Compounds **1**–**5** are insoluble in water and common organic solvents (such as methanol, ethanol and ether), and they are all stable in atmosphere.

3.2. Crystal structures

3.2.1. Structure description of (Him)$_n$[Ln(ip)$_2$(H$_2$O)]$_n$ [Ln = La(**1**), Pr(**2**), Nd(**3**) and Dy(**4**)]

The structure determinations of compounds **1**–**4** reveal that they are isostructural and crystallize in orthorhombic system, space group Pnna, herein only the structure of **1** will be discussed as a representation. The asymmetric unit of compound **1** contains one crystallographically independent lanthanum cation, two ip anions, one protonated imidazole cation and one coordinated water molecule. The coordination geometry of the La(III) center is described as a distorted tricapped trigonal prism formed by one oxygen atom (O1W) from coordinated water molecule and eight oxygen atoms (O2, O3, O4, O5, O6, O7, O8 and O9) from six symmetry-related ip ligands (Fig. 1). The La–O bond distances

range from 2.425(15) to 2.718(4) Å for **1**, Pr–O range from 2.382(2) to 2.681(3) Å for **2**, Nd–O range from 2.378(2) to 2.673(5) Å for **3** and Dy–O range from 2.287(2) to 2.604(2) Å for **4**. It can be seen that Ln–O bond lengths decrease as atomic numbers of Ln increase and this trend is in agreement with lanthanide contraction rule [23]. The coordination mode (μ_3-quadridentate) of ip ligand in compound **1** is shown in Fig. 2(a): C8 carboxyl group adopts μ_1-η^1: η^1 chelating coordination mode and C1 carboxyl group takes μ_2-η^1: η^1 bridging fashion (Scheme S1).

The most striking feature of **1** is that three different helical channels (I–III) interconnect to give a 3-D open framework (Figs. 3, 4 and S1). The helical channels I are made of left- and right-handed double helical chains ($-La-O2-C1-O3-La-$)$_n$ as walls with a pitch of 9.53 Å running along a crystallographic 2_1 screw axis in a direction (Fig. 4c), and La atoms are located at intersecting points of the left- and right-handed double helical chains. The approximate dimension of the tube is 2.89×4.53 Å^2 (Fig. S2). Channels II are formed from two intertwined single-helical chains along a axis with right-handed helicity as wall (Figs. 4b and S3), while channels III are made of two intertwined single-helical chains along a axis with left-handed helicity as wall (Figs. 4d and S3). Each single-helical chain of II and III has

Fig. 4. (a) Projection view of the helical channels (I, II and III). (b) The helical channel II with two-intertwined right-handed single-helical chains as walls. (c) The helical tube I having left- (marked as blue) and right-handed (marked as purple) double helical chains. (d) The helical channel III with two-intertwined left-handed single-helical chains as walls.

a $-La-O5-C8-C6-C7-C2-C1-O2-La-O2-C1-O3-$ repeating unit with a pitch of 19.06 Å being twice of the pitch of the double helix I. The approximate dimension of the helical channels is 3.84×12.19 Å (Fig. S2). Notably, although each double-helix II and III is a chiral one, with either left- or right-handed helicity, the whole structure is mesomeric, which originates from the equivalence of double-helices with opposite helicity. Each helical channel I connects four neighboring ones through ip ligands to generate four 1-D helical channels down a axis (two II and two III), and the helical channels I interlink with right-handed helical channels II and left-handed ones III to construct a new 3-D open framework. The protonated imidazole (Him) are filled in the helical channels II and III, and there exist strong N–H···O hydrogen bonds (N1···O4 = 2.799 Å) between N1 atom of Him (and its symmetrically relevant ones) and O4 atom (and its symmetrically relevant ones) on the inner wall of the channels II and III. The Him act as both charge compensating ions and structure-directing agent, being different from the behaviors of imidazole acting as terminal ligands in previously reported transition metal compounds constructed by ip and imidazole-mixed ligands [24–27]. It is noted that there are 2-D channels in the 3-D framework of compounds **1–4**, that is, there also exist channels down b axis (Fig. S4) besides above-mentioned channels along the a axis.

A better insight into the nature of the 3-D framework can be achieved by the application of topological approach. Each La(III) center connecting with six ip ligands is viewed as a six-connected node (Fig. 1a), correspondingly, each ip ligand coordinating to three metal centers is regarded as a three-connected node (Fig. 2a), then the two different kinds of nodes in the ratio 2:1 interconnect each other to form a 3-D (3,6)-connected network with the Schläfli symbol $(4^2.6)_2(4^4.6^2.8^7.10^2)$ (Fig. 5). Compared to the reported (3,6)-connected networks of 3-D coordination
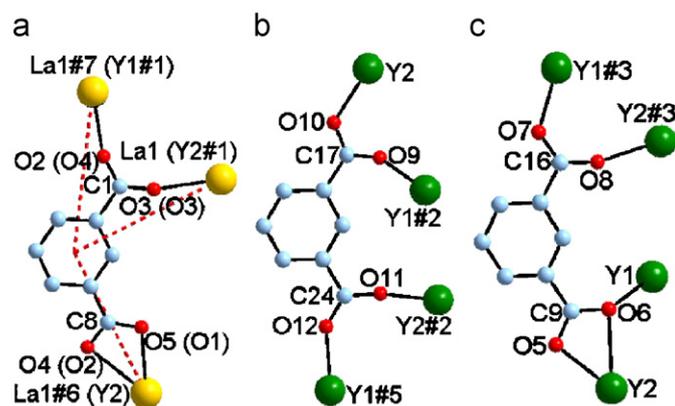

Fig. 2. Coordination modes of ip ligands in this work: (a) the mode of ip in compounds **1–4** and ip 1 in compound **5** (the atom labels of ip 1 in compound **5** are placed in the parentheses), dashed lines illustrate the three-connected circumstance of the ip node in compound **1**, (b) the mode of ip 2 and (c) the mode of ip 3 in compound **5**. Symmetry codes: #1,−x, 1−y, −z; #2, 1−x, −0.5+y, 0.5−z; #3, 1−x, 0.5+y, 0.5−z; #4, x, 1+y, z; #5, x, −1+y, z; #6, x, 0.5−y, 0.5−z; #7, 2−x, −y, −z.
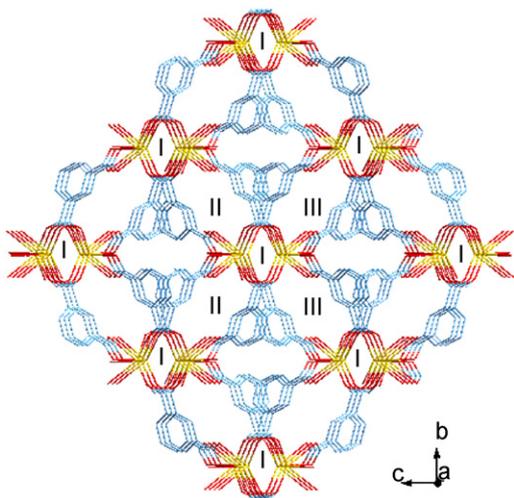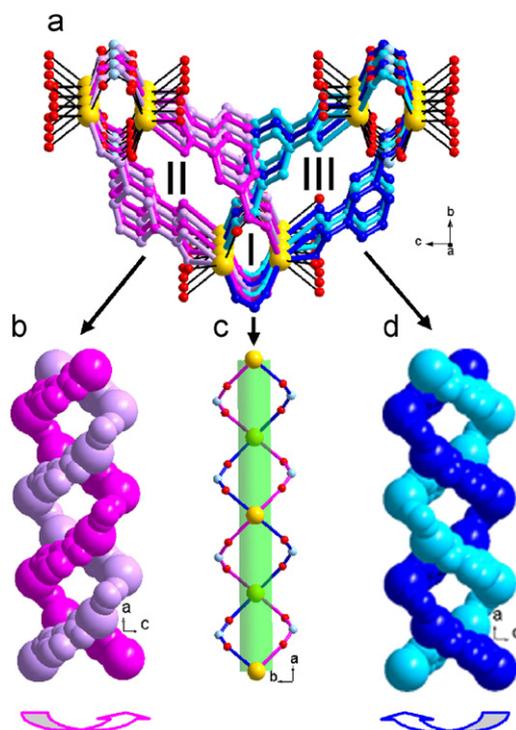

Fig. 3. A view of the 3-D framework of compound **1** running along the a axis. I/II/III: helical channels. Coordinated water molecules are omitted for clarity.

polymers [28–35], such as the rutile net with the Schläfli symbol $(4.6^2)_2(4^2.6^{10}.8^3)$, the pyrite-like network with the Schläfli symbol $(6^3)_2(6^{12}.8^3)$, the **qom** net with Schläfli symbols $(4^3)(4.6^2)(4^4.6^8.8^3)$, $(4.6^2)_2(4^2.6^9.8^4)$ and $(4.6^2)_2(4^2.6^{10}.8^3)$, and an anatase net with the Schläfli symbol $(4^2.6)_2(4^4.6^2.8^8.10)$, to the best of our knowledge, this is no example for a lanthanide coordination polymers with such a topological network.

3.2.2. Structure description of $[Y_2(ip)_3(H_2O)_2]_n \cdot nH_2O$ (**5**)

The structure determination of compound **5** reveals that it is a 2-D layer structure, crystallizing in monoclinic space group $P2_1/c$. The asymmetric unit of compound **5** contains two independent Y(III) ions, three ip ligands, two coordinated water molecules and one lattice water molecule. The three ip ligands can be just classified into three types based on their coordination modes with Y(III) ions (Fig. 2): (a) ip 1: its coordination mode is the same as that of the fashion of the ip in compounds **1**–**4** (Fig. 2a), (b) ip 2
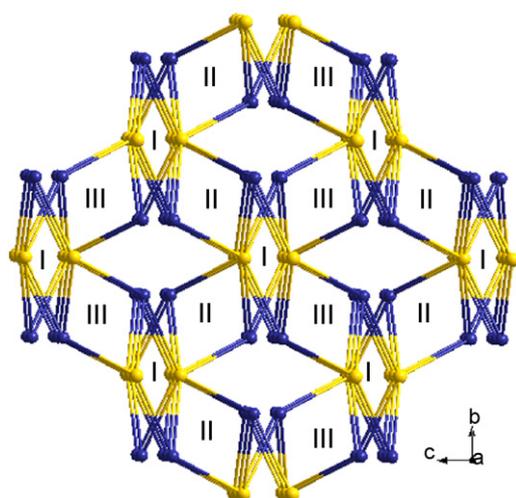

Fig. 5. Schematic representation of the (3,6)-connected topological network with the Schläfli symbol $(4^26)_2(4^46^28^710^2)$ of **1** (six-connected nodes are depicted in yellow and three-connected nodes dark blue). I/II/III: helical channels.

(μ_4-quadridentate): C17 and C24 carboxyl groups both adopt $\mu_2-\eta^1$: η^1 mode (Fig. 2b and Scheme S1) and (c) ip 3 (μ_4-pentadentate): C9 carboxyl group adopts $\mu_2-\eta^1$: η^2 mode and C16 carboxyl group is in $\mu_2-\eta^1$: η^1 fashion (Fig. 2c and Scheme S1). Coordination environments of two crystallographically different Y(III) ions (Y1(III) and Y2(III)) are shown in Fig. 6. Y1(III) is surrounded by seven oxygen atoms and has a distorted mono-capped trigonal prismatic environment (Fig. 6a and b). The seven coordination sites are occupied by O4 of C1 carboxyl group from ip 1 ligand, O9 and O12 of C17 and C24 carboxyl groups from two different ip 2 ligands, respectively, O6 and O7 of C9 and C16 carboxyl groups from two different ip 3 ligands, respectively, and O13W and O14W from two coordinated water molecules, respectively. Y2(III) is surrounded by eight oxygen atoms and takes a distorted dicapped trigonal prismatic arrangement (Fig. 6a and c): O1 and O2, chelating the Y2(III), and O3 being from C8 and C1 carboxyl groups of two ip 1 ligands, respectively, O10 and O11 being from C17 and C24 carboxyl groups of two ip 2 ligands, respectively, O5 and O6, chelating the Y2(III), and O8 being from C9 and C16 carboxyl groups of two ip 3 ligands, respectively. The Y–O bond distances are in the range 2.221(3)–2.641(3) Å. Y1(III) and Y2(III) are connected each other through O6 of C9 carboxyl group to form a vertex-shared Y2O14 dimer (Figs. 7 and S5). Then, each dimer connects two neighboring ones by ip 2 and 3 to form two kinds of infinite chains A and B along the b axis (Fig. 7a). Interestingly, both the infinite chains A and B are made up of interweaved single- and triple-helices (Figs. 8, 9, S6 and S7). For A, the single-helix is left handed and has a repeating unit of –Y2–O6–Y1–O9–C17–O10– with a pitch of 14.22 Å running along a crystallographic 2_1 screw axis in b direction (Fig. 8a and c). The triple-helix consists of three interlaced chains (Fig. 8b and c). Each strand of the triple-helix is right-handed and has a repeating unit of –Y2–ip3–Y1–ip2–. The pitch of each strand is 42.65 Å, which is three times of that of the single-helix. The triple-helix inter-weaves with the single-helix across –Y1–O9–C17–O10– (Fig. 8c). But for B, the helicity of either single-helix or triple-helix is opposite to that of A (Figs. 9 and S7). In fact, A and B chains are symmetry equivalent. It is noteworthy that there exist simultaneously two kinds of quadruple-helices A and B, which
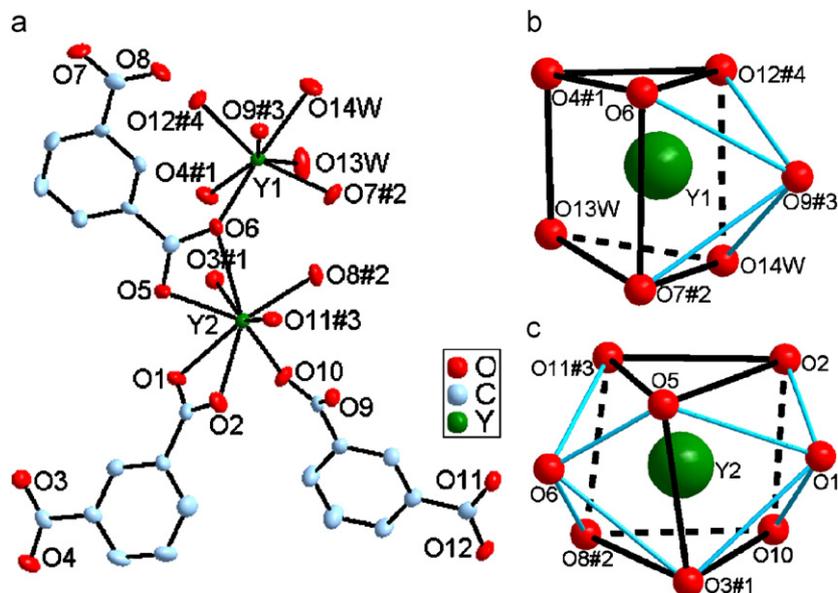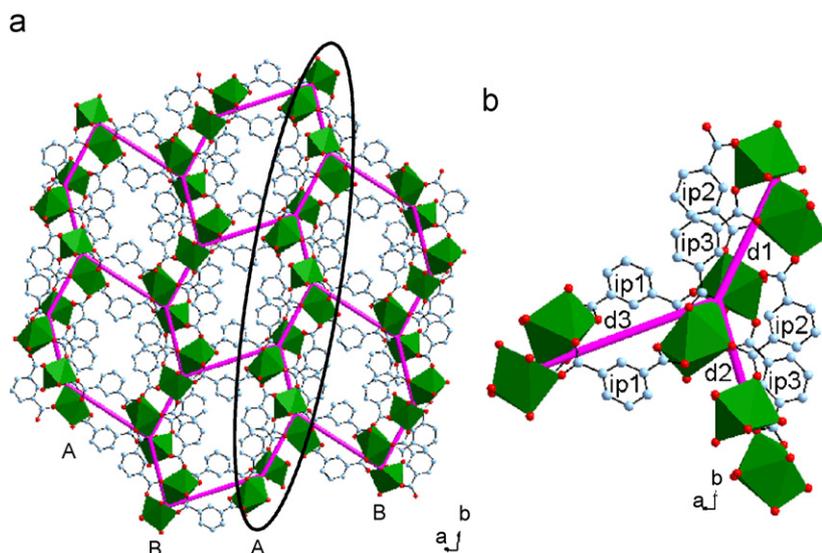

Fig. 6. (a) Coordination environments of Y1(III) and Y2(III) in compound **5**. Thermal ellipsoids are at 50% probability. (b) The distorted monocapped trigonal prismatism coordination polyhedron of the Y1(III) ion. (c) The distorted dicapped trigonal prismatism coordination polyhedron of the Y2(III) ion. Symmetry codes: #1, −x, 1−y, −z; #2, 1−x, −0.5+y, 0.5−z; #3, 1−x, 0.5+y, 0.5−z; #4, x, 1+y, z.

Fig. 7. (a) A view of the 2D honeycomb-like structure (ellipse part shows the infinite chain A) of compound **5**. (b) The representation of a three-connected node in compound **5**.
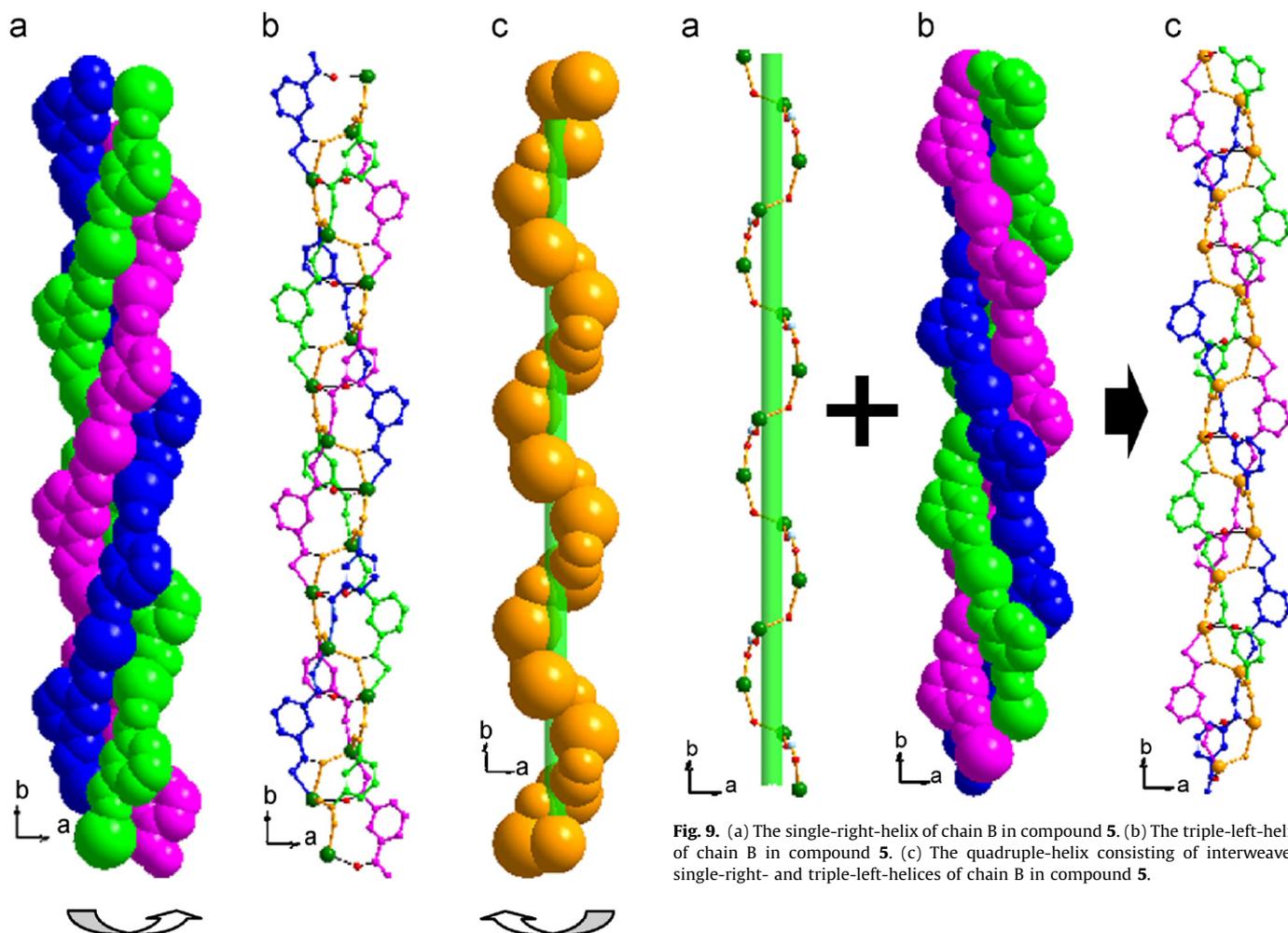

Fig. 8. (a) The triple-helix marked as blue, purple and green of chain A in compound **5**. (b) The interweaved triple- and single-helices of chain A in compound **5**. (c) The single-helix marked as orange of chain A in compound **5**.

Fig. 9. (a) The single-right-helix of chain B in compound **5**. (b) The triple-left-helix of chain B in compound **5**. (c) The quadruple-helix consisting of interweaved single-right- and triple-left-helices of chain B in compound **5**.

consist of intertwined single-left- and triple-right-helices, and single-right - and triple-left-helices, respectively. This situation is very rare in reported relevant literatures so far.

Adjacent A and B are interconnected through ip 1 to form a honeycomb-like 2-D layer structure along *ab* plane (Fig. 7a). The lattice water molecules are situated on both side of the layer along *b* axis (Fig. S8). There are extensive intramolecular hydrogen bonds among the coordinated water molecules, lattice water and the oxygen atoms of ip 1 ligand (O14W···O2, 2.711 Å; O14W···O15W, 3.262 Å and O13W···O15W, 2.708 Å). These weak

interactions play important roles in the stabilization of the layer structure of **5**. *Via* hydrogen bonds (O13W···O10, 2.747 Å and O15W···O1, 2.919 Å), the 2-D layers are linked into a 3-D supramolecular network (Fig. S9).

In the view of topology of compound **5**, each Y_2O_{14} dimer serving as a three-connected node connects three neighboring ones to form a 2-D honeycomb-like topological layer with the Schläfli symbol 6^3 (Fig. 7a). The dimer···dimer separation across the ip 2 and 3 bridges is 7.64 Å (d1 and d2), and across the ip 1 bridges (d3) 10.92 Å (Fig. 7b). If hydrogen bonding interactions are taken into account, the dimer becomes a 4-connected node and the network turns into a 4-connected topological network with the Schläfli symbol 6^6 (Fig. 10). This network is different from that of the diamond net in which 4-connected node possessing an ideal tetrahedral connection configuration.

In a comparison of previously reported 2-D layer structures constructed by lanthanides and isophthalate ligands and compound **5**, it is found that the coordination modes of isophthalate ligands are different. In the former, there are two coordination modes (μ_5-heptadentate and μ_4-pentadentate) of isophthalate ligands in $[K_2Eu_2(ipa)_4(H_2O)_4 \cdot 8H_2O]$ [12], two coordination modes (μ_4-pentadentate and μ_4-quadridentate) of ones in $[Nd_2(ip)_3(H_2O)_2]_n$ and $[Gd_2(ip)_3(H_2O)_2]_n$ [13], and three coordination modes (μ_4-pentadentate, μ_4-hexadentate and μ_2-tridentate) of ones in $[La_2(isophth)_2(Hisophth)_2(H_2O) \cdot H_2O]_n$ [14], respectively. While in compound **5**, there are three different coordination modes of ones: μ_3-quadridentate being unprecedented, μ_4-quadridentate and μ_4-pentadentate.

3.3. IR spectra

The main IR bands with their tentative assignments of compounds **1**–**5** are summarized in Table 3. For isostructural compounds **1**–**4**, the observed bands of 3630 and 3430 cm⁻¹ char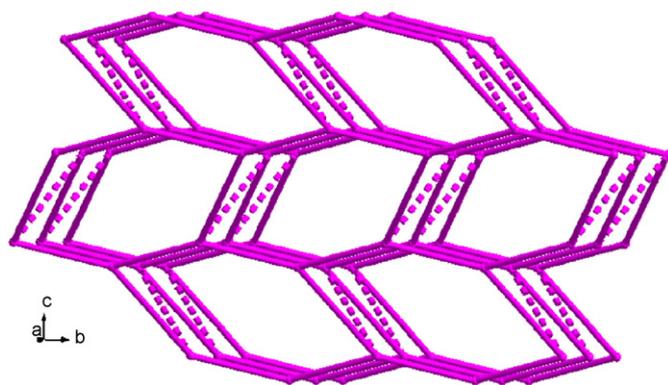acterize water molecules in the structures. The bands of N–H of imidazole stretch at 3180–3060 cm⁻¹, while the bands of C–H of aromatic rings at 2989–2860 cm⁻¹. Strong bands of 1650–1540 cm⁻¹ are characteristic of asymmetric stretching vibration of carboxylate groups, and the bands at about 1650 cm⁻¹ should involve the vibration of C=C or C=N. The strong bands appear at about 1390 cm⁻¹ due to the symmetric stretching vibration of carboxylate groups. For compound **5**, the broad band of 3510–3220 cm⁻¹ characterizes water molecules in the structure, although this band may contain weak C–H stretching vibration. Asymmetric and symmetric stretching vibrations of carboxylate groups are observed at 1532 and 1395 cm⁻¹, respectively.

3.4. UV–Vis–NIR spectroscopy

The UV–Vis–NIR diffusion reflection spectrum in solid state (Fig. 11) of compound **2** exhibits the *f–f* electronic transitions of Pr(III) ions from the $^4H_3$ ground level to $^3P_2$ (445 nm), $^3P_1$ (471 nm), $^1D_2$ (593 nm), $^1G_4$ (993 nm), $^3F_4$ (1408 nm) and $^3F_3$ (1511 nm) levels according to the energy diagram of trivalent lanthanide elements [36]. The strong absorption below 350 nm can be assigned to the organic linker's π–π transitions.

Compound **3** shows well UV–Vis–NIR diffusion reflection spectrum in solid state (Fig. 12). The strong absorption band below 365 nm is ascribed to the organic linker's π–π transitions, while the absorption bands above 365 nm can be readily assigned to the corresponding *f–f* electronic transitions of the Nd(III) ions from the ground state to the excited states $^4F_{3/2}$ (870 nm), $^4F_{5/2}$ (800 nm), $^4F_{7/2}$ (747 nm), $^4F_{9/2}$ (683 nm), $^2H_{11/2}$ (630), $^2G_{7/2}$ (585 nm), $^4G_{7/2}$ (524 nm), $^2G_{9/2}$ (461 nm) and $^4G_{11/2}$ (430 nm).
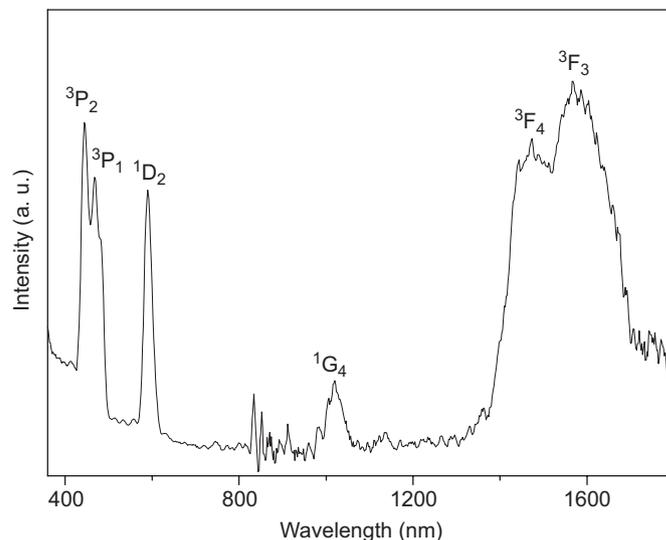

Fig. 10. Schematic representation of the 3-D 6^6 supramolecular topology of compound **5** (hydrogen bonds are depicted as dashed lines).

Fig. 11. Diffuse reflectance spectrum of compound **2** in solid state.

Table 3
IR absorption bands (cm⁻¹) and their assignments for compounds **1**–**5**

Vibrations	1	2	3	4	5
νOH	3630w, 3480w	3610w, 3480w	3620w, 3480w	3600w, 3479w	3510–3220m
νN–H	3180–3070m	3180–3068m	3178–3070m	3179–3069m	
νC–H	2989–2860m	2988–2860m	2988–2860m	2985–2860m	
ν_sCOO, νC=C/C=N	1646–1544s	1650–1548s	1651–1551s	1661–1550s	1620–1532s
ν_{as}COO	1386s	1386s	1388s	1392s	1395s
δCH	851w, 744m	852w, 744m	851w, 744m	851w, 744m	835w, 746m

s, strong; m, medium; w, weak; ν, stretching vibration; ν_s, symmetric stretching vibration; ν_{as} asymmetric stretching vibration; δ, deformation.

3.5. Luminescence properties

It is well known that the direct excitation produces only weak emission spectra due to the low molar absorption coefficients of the lanthanides. The mechanism of energy transfer in molecules is always one of the important subjects of research on photoluminescence coordination compounds. In some reported mechanism of energy transfer, the mechanism presented by Whan and Crosby has been so far the most successful one in explaining "antenna effect" [37]. First of all, π electron of the ligand is directly excited to a singlet state S1 of lowest excitation state from the singlet state S0 of ground state via $\pi^* \leftarrow \pi$ absorption followed by an intersystem crossing to a triplet state T1 of lowest excitation state. Then the ground state electron of the lanthanide ion is excited and transits to an excitation state, when the energy is transferred from triplet state T1 to the lanthanide ion. The lanthanide ion thus emits characteristic luminescence when the electron transits back to ground state of lanthanide ion. This effect is commonly known as "antenna effect" [38]. The ip ligand used in the formation of the compounds absorbs strongly in the UV region (Fig. S10) and it is an attractive ligand for sensitizing Pr, Nd and Dy via the antenna effect.

The luminescence spectrum of Pr(III) are more complicated in comparison with those of other lanthanide systems such as Nd(III) ions, as Pr(III) can show emission lines originating from three different levels ($^3P_0$, $^1D_2$ and $^1G_4$) upon excitation of the organic ligands' absorption [39]. Since radiative transitions are more likely to occur when energy gaps are larger, transitions from the $^1D_2$ level are more liable than transitions from the $^3P_0$ level or the $^1G_4$ level. The observed NIR emission spectrum of compound **2** consists of three bands when excited at 488 nm (Fig. 13): the strongest emission band from 960 to 1100 nm with $\lambda_{max} = 1030$ and $\lambda_{max} = 993$ nm attributing to $^1D_2 \rightarrow {}^3F_4$ and $^1D_2 \rightarrow {}^3F_3$ transitions, respectively; the band between 830 and 900 nm attributing to the $^1D_2 \rightarrow {}^3F_2$ transition; the band between 1400 and 1500 nm attributing to the $^1D_2 \rightarrow {}^1G_4$ transition [40]. The absence of emission at around 1320 nm corresponding to $^1G_4 \rightarrow {}^3H_3$ indicates that the nonradiative process with phonon assistance dominates the relaxation of $^1G_4$ manifold energy levels. Therefore, emitting peaks at 993 and 1030 nm are originated from $^1D_2$, not $^1G_4$. By using such Ln(III) ions, the spectral
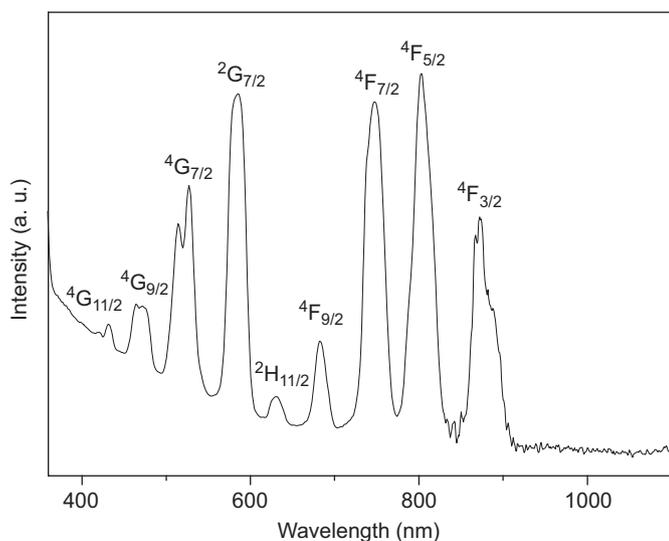
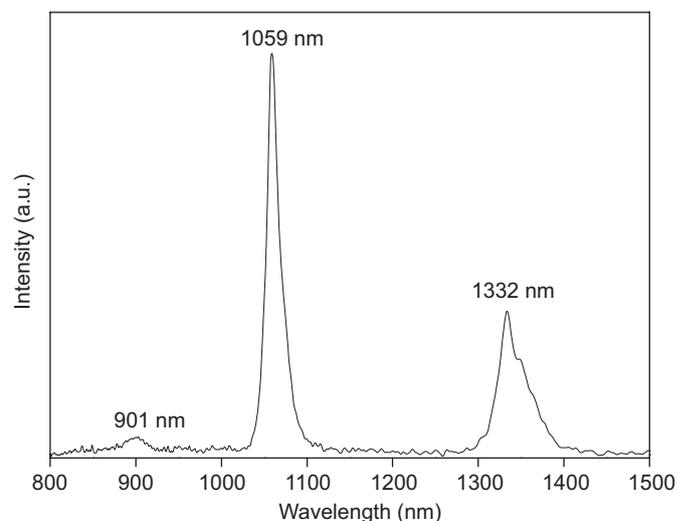**Fig. 12.** Diffuse reflectance spectrum of compound **3** in solid state.

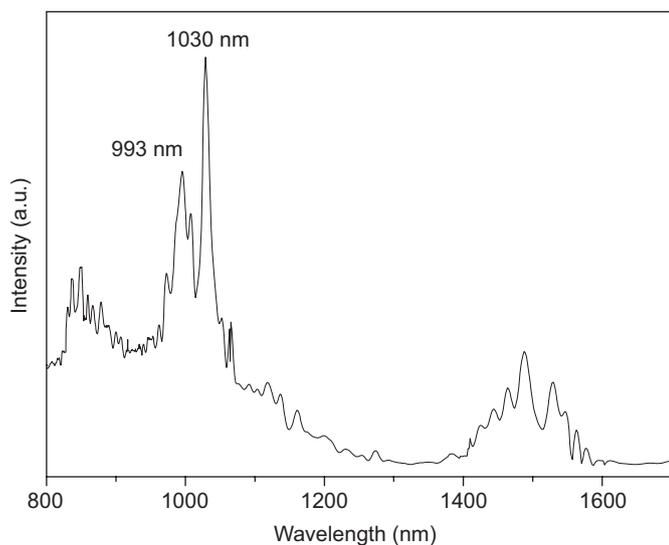**Fig. 14.** Solid-state emission spectrum ($\lambda_{ex} = 488$ nm) of compound **3** in the NIR region.

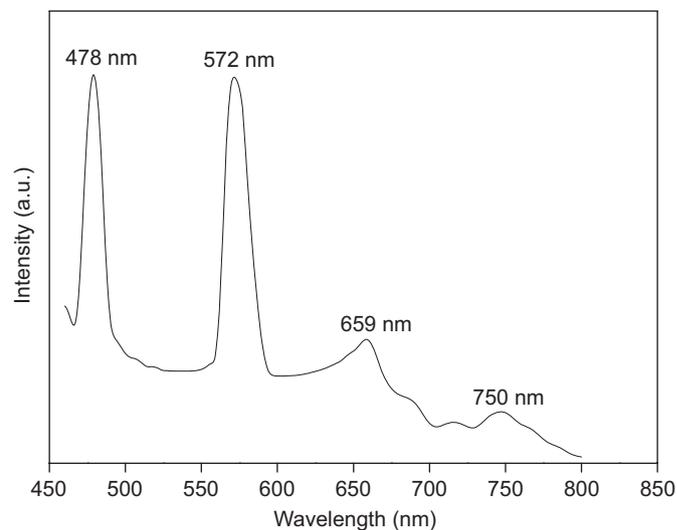**Fig. 13.** Solid-state emission spectrum ($\lambda_{ex} = 488$ nm) of compound **2** in the NIR region.

Fig. 15. Solid-state emission spectrum ($\lambda_{ex} = 300$ nm) of compound **4**.

region from 1300 to 1600 nm, which is of particular interest for telecommunication applications, can be covered completely.

Compound **3** shows the characteristic emission bands in the NIR region (Fig. 14) for the Nd(III) ion when excited at 488 nm: the three bands at $\lambda = 901$, 1059 and 1332 nm are attributed to the f–f transitions $^4F_{3/2} \rightarrow ^4I_{9/2}$, $^4F_{3/2} \rightarrow ^4I_{11/2}$ and $^4F_{3/2} \rightarrow ^4I_{13/2}$, respectively. Among the three bands of the Nd(III) compound, the intensity of the transition at 1059 nm is the strongest and potentially applicable for laser emission.

Upon excitation at 300 nm in the solid state at room temperature, compound **4** emit strong characteristic luminescence for the Dy(III) ions (Fig. 15). There are four emission bands in the visible region, two strong bands at 478 and 572 nm and two weaker bands at 659 and 750 nm, which can be assigned to $^4F_{9/2} \rightarrow ^6H_{15/2}$, $^4F_{9/2} \rightarrow ^6H_{13/2}$, $^4F_{9/2} \rightarrow ^6H_{11/2}$, $^4F_{9/2} \rightarrow ^6H_{9/2}$ of the Dy(III) ions, respectively.

4. Conclusion

In summary, a series of lanthanide coordination polymers constructed by isophthalate have been synthesized by hydrothermal reactions and structurally characterized by single-crystal X-ray diffraction analyses. Isostructural compounds **1**–**4** possess 3-D frameworks consisting of three different kinds of helical channels. Compound **5** displays a 2-D honeycomb-like network making of two kinds of quadruple-helical chains and it turns out to be 4-connected topological network with the Schläfli symbol 6^6 when hydrogen bonds are considered. The structures of these compounds verify that high and variable coordination numbers and flexible coordination environment of lanthanide ions suit the formation of coordination polymers possessing various structures. Compounds **2** and **3** show the characteristic emissions of Pr(III) and Nd(III) ions in the NIR region, respectively. Compound **4** displays sensitized luminescence of Dy(III) in the visible region.

Supplementary materials

CCDC ⟨660382-6603806⟩ contains the supplementary crystallographic data for ⟨**1**–**5**⟩. These data can be obtained free of charge via http://www.ccdc.cam.ac.uk/conts/retrieving.html, or from the Cambridge Crystallographic Data Centre, 12 Union Road, Cambridge CB2 1EZ, UK; fax: (+44) 1223-336-033; or e-mail: deposit@ccdc.cam.ac.uk.

Acknowledgment

Appendix A. Supplementary materials

The online version of this article contains additional supplementary data. Please visit doi:10.1016/j.jssc.2008.05.011

References

[1] B. Moulton, M.J. Zaworotko, Chem. Rev. 101 (2001) 1629–1658.
[2] N.L. Rosi, J. Echert, M. Eddaoudi, D.T. Vodal, J. Kim, M. O'Keeffe, O.M. Yaggi, Science 300 (2003) 1127–1129.
[3] O.M. Yaghi, H. Li, C. Davis, D. Richardson, T.L. Groy, Acc. Chem. Res. 31 (1998) 474–484.
[4] C.N. Rao, S. Natarajan, R. Vaidhyanathan, Angew. Chem. Int. Ed. 43 (2004) 1466–1496.
[5] S.R. Batten, B.F. Hoskins, B. Moubaraki, S. Murray, K.R. Robson, Chem. Commun. (2000) 1095–1096.
[6] B.L. Chen, Y. Yang, F. Zapata, G.D. Qian, Y.S. Luo, J.H. Zhang, E.B. Lobkovsky, Inorg. Chem. 45 (2006) 8882–8886.
[7] D.L. Long, A.J. Blake, N.R. Champness, C. Wilson, M. Schröder, J. Am. Chem. Soc. 123 (2001) 3401–3402.
[8] J.P. Zhang, Y.Y. Lin, X.C. Huang, X.M. Chen, J. Am. Chem. Soc. 127 (2005) 5495–5506.
[9] O. Guillou, C. Daiguebonne, Handbook on the Physics and Chemistry of Rare Earths, Elsevier Science, Amsterdam, 2004.
[10] X.M. Chen, G.F. Liu, Chem. Eur. J. 8 (2002) 4811–4817.
[11] E. Psillakis, J.C. Jeffery, J.A. McCleverty, M.D. Ward, Chem. Commun. (1997) 479–480.
[12] A.D.B. Dias, Inorg. Chem. 44 (2005) 2734–2741.
[13] Y.F. Zhou, F.L. Jiang, Y. Xu, R. Cao, M.C. Hong, J. Mol. Struct. 691 (2004) 191–195.
[14] D.X. Hu, P.K. Chen, F. Luo, Y.X. Che, J.M. Zheng, J. Mol. Struct. 837 (2007) 179–184.
[15] Y.H. Wan, L.P. Zhang, L.P. Jin, J. Mol. Struct. 658 (2003) 253–260.
[16] Y.F. Zhou, F.L. Jiang, D.Q. Yuan, B.L. Wu, R.H. Wang, Z.Z. Lin, M.C. Hong, Angew. Chem. Int. Ed. 43 (2004) 5665–5668.
[17] Y.F. Zhou, D.Q. Yuan, F.L. Jiang, Y.Q. Xu, M.C. Hong, J. Mol. Struct. 796 (2006) 203–209.
[18] A. Thirumurugan, S. Natarajan, Dalton Trans. (2004) 2923–2928.
[19] X.J. Zheng, T.T. Zheng, L.P. Jin, J. Mol. Struct. 740 (2005) 31–35.
[20] B. Kesanli, W. Lin, Coord. Chem. Rev. 246 (2003) 305–326.
[21] G.M. Sheldrick, SHELXS 97, Program for Crystal Structure Refinement, University of Göttingen, Göttingen, Germany, 1998.
[22] A.L. Spek, PLATON, Molecular Geometry Program, University of Utrecht, The Netherlands, 1999.
[23] L. Pan, X. Huang, J. Li, Y. Wu, N. Zheng, Angew. Chem. Int. Ed. 39 (2000) 527–530.
[24] C.B. Ma, C.N. Chen, Q.T. Liu, F. Chen, D.Z. Liao, L.C. Li, L.C. Sun, Eur. J. Inorg. Chem. (2004) 3316–3325.
[25] J.F. Song, Y. Chen, Z.G. Li, R.S. Zhou, X.Y. Xu, J.Q. Xu, J. Mol. Struct. 842 (2007) 125–131.
[26] L.B. Wang, X.M. Li, Q.W. Wang, B. Liu, Acta Crystallogr. E 63 (2007) m715–m716.
[27] J.H. Yang, S.L. Zheng, J. Tao, G.F. Liu, X.M. Chen, Aust. J. Chem. 55 (2002) 741–744.
[28] S.R. Batten, P. Jensen, B. Moubaraki, K.S. Murray, R. Robson, Chem. Commun. (1998) 439–440.
[29] J. Kim, B. Chen, T.M. Reineke, H. Li, M. Eddaoudi, D.B. Moler, M. O'Keeffe, O.M. Yaghi, J. Am. Chem. Soc. 123 (2001) 8239–8247.
[30] P. Jensen, D.J. Price, S.R. Batten, B. Moubaraki, K.S. Murray, Chem. Eur. J. 6 (2000) 3186–3195.
[31] E.Y. Lee, S.Y. Jang, M.P. Suh, J. Am. Chem. Soc. 127 (2005) 6374–6381.
[32] L.G. Beauvais, M.P. Shores, J.R. Long, Chem. Mater. 10 (1998) 3783–3786.
[33] D.J. Chesnut, D. Plewak, J. Zubieta, J. Chem. Soc. Dalton Trans. (2001) 2567–2580.
[34] S.C. Xiang, X.T. Wu, J.J. Zhang, R.B. Fu, S.M. Hu, X.D. Zhang, J. Am. Chem. Soc. 127 (2005) 16352–16353.
[35] H.K. Chea, D.Y.S. Pérez, J. Kim, Y. Go, M. Eddaoudi, A.J. Matzger, M. O'Keeffe, O.M. Yaghi, Nature 427 (2004) 523–527.
[36] G.H. Dieke, Spectra and Energy Levels of Rare Earth Ions in Crystals, Interscience Publishers, New York, 1968.
[37] R.E. Whan, G.A. Crosby, J. Mol. Spectrosc. 8 (1962) 315–327.
[38] B.D. Chandler, D.T. Cramb, G.K.H. Shimizu, J. Am. Chem. Soc. 128 (2006) 10403–10412.
[39] A.I. Voloshin, N.M. Shavaleev, V.P. Kazakov, J. Lumin. 93 (2001) 199–204.
[40] S. Comby, J.C.G. Bünzli, Handbook on the Physics and Chemistry of Rare Earths, Elsevier Science, Amsterdam, 2007.